ACS OMEGA

Open Access

http://pubs.acs.org/journal/acsodf

Article

Macrophage Responses to Multicore Encapsulated Iron Oxide Nanoparticles for Cancer Therapy

Sarah Kraus,* Shir Arbib, Pazit Rukenstein, Irit Shoval, Raz Khandadash, and Ofer Shalev

Cite This: *ACS Omega* 2025, 10, 3535−3550

Read Online

ACCESS | Metrics & More | Article Recommendations

ABSTRACT: Macrophages are the primary cells responsible for nanoparticle processing and mediating host immunological biological outcomes. Their cellular response to nanoparticles is a vital constituent in the safety assessment of new designs for clinical application. An approach for the treatment of solid tumors was developed, based on magnetic hyperthermia, consisting of iron oxide multicore encapsulated nanoparticles named Sarah nanoparticles (SaNPs), and alternating magnetic field irradiation. SaNPs are intravenously injected, accumulate in the liver, spleen and in tumor tissue, where they are passively targeted to malignant cells via the Enhanced Permeability and Retention (EPR) effect and undergo selective heating. SaNP-induced responses after cellular uptake were investigated in murine RAW264.7 macrophages using a wide imaging approach. When activated, macrophages form different phenotypic populations with unique immune functions, however the mechanism/s by which these activated macrophages respond to nanoparticles is unclear. Unraveling these responses is important for the understanding of nanoparticle uptake, potential degradation, and clearance to address both toxicity and regulatory concerns, which was the aim of this study. The results demonstrated that SaNPs undergo internalization, localize within the lysosomal compartment while keeping their integrity, without intracellular toxic degradation, and are cleared with time. The production of tumor necrosis factor alpha (TNF-α) and reactive oxygen species (ROS), superoxide dismutase (SOD) activation, and cytokine secretion in macrophage conditioned medium (CM) were also evaluated. SaNPs effects were both time- and dose- dependent. High SaNP concentrations resulted in reduced RAW264.7 cell viability which correlated with SOD activation and was associated with ROS generation. Lower SaNP concentrations stimulated the time-dependent production of TNF-α. The expression of additional cytokines was also induced, potentially affecting cancer cell growth by CM from SaNP-activated macrophages supporting a potential antitumor effect. These results will help understand the fate of nanoparticles in vivo.

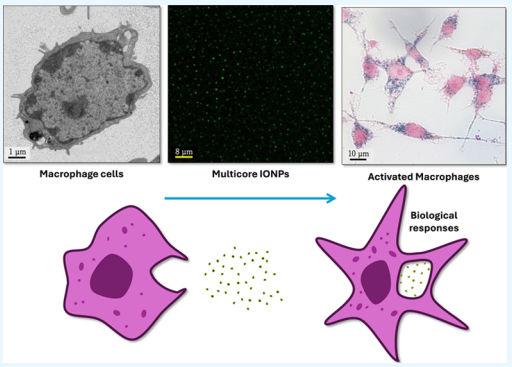

1. INTRODUCTION

The development of nanoparticle-based therapeutics offers novel technologies for the treatment of cancer and particularly regarding hyperthermia using magnetic nanoparticles.[1] The unique size and physicochemical characteristics of nanoparticles, including surface composition, charge, and shape, pose several advantages such as the ability to undergo surface modification rendering improved pharmacokinetics, biocompatibility, uptake efficiency, and reduced toxicity.[2]

We have developed an approach for the treatment of stage IV metastatic solid tumors, comprising of multicore encapsulated iron oxide (IO) Sarah Nanoparticles (SaNPs) and an Electromagnetic Induction System (EIS). The Sarah Nanotechnology approach, named after a patient who died of lung cancer, is currently being investigated in a first-in-human clinical trial in patients with metastatic solid tumors (MoH_2022-09-18_012060). SaNPs were generated using an emulsification-evaporation method as previously described, yielding a monodispersed colloid.[3] IO nanoparticles such as magnetite (Fe_3O_4) or its oxidized form maghemite (Fe_2O_3) are widely used for in vivo biomedical applications. Magnetite-based SaNPs contain amine functionalized 6-arm-branched polyethylene glycol (PEG) 20,000-encapsulated IO nanoclusters and a phase change material (PCM) core, with a size ranging between 90 and 165 nm with narrow size distribution and negative zeta potential values within the range of (−5)−(−30) mV.[4] SaNPs are intravenously injected, accumulate in tumors and metastases, due to the enhanced permeability and retention (EPR) effect, a pathophysiological phenomenon that enables the extravasation of nanoparticles through permeable tumor vessels and their retention into solid tumors characterized by reduced lymphatic drainage. SaNPs then

Received: August 27, 2024
Revised: December 25, 2024
Accepted: January 13, 2025
Published: January 22, 2025

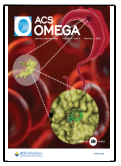

undergo selective heating in the presence of an externally applied alternating magnetic field (AMF) generated by the EIS, consequently inducing cancer cell death at subablative temperatures of up to 50 ± 3 °C.

SaNPs uniquely self-regulate their temperature owing to the PCM properties whereas the PEG 20,000 component serves as an encapsulating hydrophilic polymer that enables nanoparticle flexibility, increases biocompatibility, and significantly masks the SaNPs from the body's mononuclear phagocyte system (MPS), thereby reducing uptake by phagocytic cells. Polymer encapsulation is also aimed at preventing structural changes, aggregation, and biodegradation when exposed to the biological environment. The accumulation of SaNPs and attaining a thermal mass in the tumor site are required for their therapeutic effect. However, potential accumulation in normal tissues and associated toxicity must be considered in risk analyses.

We have previously demonstrated that SaNPs accumulate in cells of the MPS, mainly liver macrophages (e.g., Kupffer cells), alveolar and splenic tissue-resident macrophages, are cleared from the body in a time-dependent manner once systemically administered to animals and are mostly eliminated in the feces through the hepatobiliary route.[4,5] SaNPs have shown lack of toxicity in animal studies in rodents and swine and were proven safe and biocompatible in these models. Unraveling their fate, clearance, and potential degradation in professional phagocytic cells, such as macrophages, is essential for understanding both their biosafety and application in cancer therapy. The fate of nanoparticles is also important for regulatory requirements dealing with concerns on chronic accumulation and patient safety. Moreover, the FDA requires nanoparticles to be metabolized or excreted from the body to be used in the clinical setting.[6]

Macrophages are the primary cells responsible for nanoparticle processing and mediating host immunological biological outcomes. Tissue-resident macrophages such as Kupffer cells and alveolar macrophages in the lungs play essential roles in local immune responses and in maintaining internal homeostasis.[7] When nanoparticles are systemically administered, they are rapidly eliminated from the circulation and accumulate mainly in the liver and spleen, due to opsonization and macrophage recognition, followed by endocytic processes. The nanoparticles then undergo internalization by various mechanisms. During their cellular uptake, nanoparticles can also undergo interaction with subcellular components, resulting in the stimulation of various cellular mechanisms that may elicit stress responses such as generation of free radicals, organelle damage, and cell death, collectively known as oxidative stress.[8] Activated macrophages rapidly generate cytokines, and reactive oxygen species (ROS) through the nicotinamide adenine dinucleotide phosphate (NADPH) oxidase pathway to promote foreign material degradation.[9] Mechanistic studies have shown that after activation, the NADPH oxidase enzyme system assembles at the phagolysosomal membrane and forms superoxide anions, which are then catalyzed by superoxide dismutase (SOD), preventing the accumulation of superoxide that can damage and cause protein inactivation. Thus, accumulation of superoxide is directly associated with oxidative stress.

Microscopy remains one of the most utilized techniques to study nanoparticles, particularly for in vitro investigation. Studies have indicated that the main destination of nanoparticles in macrophages is degradation.[10] Most of these studies have been performed in macrophage models using fluorescently tagged nanoparticles that due to their size offer a large surface area-to-volume ratio, making their application in cellular imaging useful.

The purpose of this study was to investigate the potential biodegradation and clearance of multicore IO-based SaNPs as well as the in vitro responses of murine RAW264.7 macrophage cells following their uptake and endocytosis, as part of their safety assessment, and to address regulatory concerns. To achieve this, we used a wide imaging approach, including confocal microscopy, imaging flow cytometry, and transmission electron microscopy, and further evaluated the SaNP-induced cellular effects by measuring the production of specific cytokines such as tumor necrosis factor alpha (TNF-α), the activation of SOD, and the generation of ROS. The role of conditioned medium (CM) from SaNP-activated macrophages on cancer cell proliferation was also examined suggesting a potential antitumor effect.

We believe that our results will help understand the fate of similar nanoparticles intended for clinical use. Our goal is to support the development of innovative treatments by providing evidence for their safety.

2. EXPERIMENTAL SECTION

2.1. Materials. Commercially available materials and reagents included the following: Aspartate aminotransferase (AST), bovine serum albumin (BSA), glutaraldehyde, Fluoroshield mounting media, phosphate buffered saline (PBS, pH 7.4), β-mercaptoethanol (β-ME), paraformaldehyde (PFA), phenylmethylsulfonyl fluoride (PMSF), sodium cacodylate, Triton X-100, xanthine oxidase, and 4′,6-diamidine-2′-phenylindole dihydrochloride (DAPI) were purchased from Sigma-Aldrich, Rehovot, Israel. Fetal Bovine Serum (FBS), 0.25% trypsin−EDTA solution, and antibiotics (penicillin, streptomycin) were all from Biological Industries, Beit-Haemek, Israel. Water for injection (WFI) was from B. Braun Medical Inc., PA, USA. Puromycin was purchased from Santa Cruz Biotechnology, Inc. All other chemicals used were of analytical grade. Aqueous solutions were prepared with deionized water.

2.2. Physicochemical Characterization of SaNPs. SaNPs were characterized by dynamic light scattering (DLS) and transmission electron microscope (TEM) imaging to determine their physicochemical characteristics and morphology as previously described.[4] Hydrodynamic size, size distribution, and zeta potential measurements were conducted using a Zetasizer nano-ZS (Malvern Panalytical, Malvern, UK).

2.3. Preparation of SaNPs and FITC-Labeled SaNPs. Before addition of SaNPs to the cells, the stock solution was sonicated in a water bath for 6 min to distribute the nanoparticles as homogeneously as possible. The SaNP dispersion was subsequently diluted with the cell culture medium as indicated in the individual experiments to achieve the nominal concentrations. Fluorescent labeling of SaNPs was performed by cross-linking of amine-functionalized SaNP with sulfosuccinimidyl 4-(*N*-maleimidomethyl) cyclohexane-1-carboxylate (sulfo-SMCC, ProteoChem Inc., USA) and subsequent conjugation of fluorescein-polyethylene glycol-thiol (FITC-PEG-SH), MW 1k (cat. no.: PBL-8171, Creative PEGWorks, USA) through a maleimide−thiol reaction. The procedure for the preparation of FITC-labeled SaNP was as follows: sodium bicarbonate (Merck, Israel) was dissolved in a SaNP dispersion (1.83 mg/mL) and shaken on an orbital

https://doi.org/10.1021/acsomega.4c07883
ACS Omega 2025, 10, 3535−3550

shaker for 30 min at room temperature. Then, 50 mg of sulfo-SMCC (0.11 mmol) was added to the SaNP dispersion (pH 8.35), and the mixture was further shaken for 24 h, followed by 3 washes with WFI by a precipitation-redispersion process using centrifugation (7000*g*, 1 h). After the final washing step, the maleimide-activated SaNP was dispersed in WFI using a sonication bath and reacted with 500 mg of FITC-PEG-SH (0.1 mmol) at room temperature for 24 h with shaking. The mixture was then extensively washed with WFI by a precipitation-redispersion process and further centrifugation, to remove the unbound excess of FITC-PEG-SH. The supernatant was monitored by UV to verify that no free fluorescent reagent remained in the solution. The FITC-labeled SaNP was resuspended in the original volume and filtered through a 0.2 μm cellulose acetate glass-fiber filter (Sartorius, Biological Industries, Israel) in a laminar hood to obtain a sterile FITC-labeled SaNP dispersion for cell culture experiments. The FITC-labeled SaNP was analyzed by confocal microscopy using a Leica TCS SP8 STED scanning confocal system and we verified that no free dye was released from the FITC-labeled SaNP dispersion before applying to the cells. Data acquisition was performed using the Leica Application Suite X (LASX) software (Leica Microsystems, Mannheim, Germany).

2.4. Cell Culture. Murine RAW264.7 macrophage (ATCC TIB-71) and 4T1 mammary carcinoma (ATCC CRL-2539) cell lines were obtained from the American Type Culture Collection (Rockville, MD, USA). RAW264.7 cells were grown as a monolayer in Dulbecco's Modified Eagle's Medium (DMEM) (Sartorius, Biological Industries, Israel) supplemented with 10% FBS (v/v), 100 mg/mL streptomycin, and 100 U/mL penicillin. Confluent cells were sub-cultured by scraping and seeded as described for the corresponding experiments. Cells were incubated overnight for attachment and the medium was replaced with fresh SaNP-containing culture medium. 4T1 cells were grown in RPMI 1640 medium (Sartorius, Biological Industries, Israel) supplemented with 10% (v/v) FBS, 1.0 mM sodium pyruvate, 100 μg/mL streptomycin, and 100 U/mL penicillin. All cells were maintained in a humidified atmosphere of 95% air and 5% CO_2 at 37 °C. For imaging purposes of 4T1 cells, modified human embryonic kidney GP2-293 cells were cotransfected with pRetroQ-mCherry-N1 Vector using the complementary Retro-X Universal system (Clontech, CA, USA) to generate mCherry containing viral particles. pRetroQ-mCherry-N1 retroviral particles containing supernatant were collected 48 h after transfection. 4T1 cells were infected and mCherry positive cells were selected by Puromycin (2 μg/mL) resistance.

2.5. In Vivo Study and Histological Evaluation. To examine the accumulation of SaNPs in the liver, SaNPs (1.92 mg IO/mL) were intravenously injected into 7−8 weeks old BALB/c female mice (Harlan Laboratories, Israel). The dose volume administered to the mice was 10 mL/kg. The mice were sacrificed 3 days after treatment to evaluate SaNP accumulation and potential acute toxicity effects. Untreated mice served as controls. Groups included 5 mice per group. All animal experiments were reviewed and approved by an Institutional Animal Care and Use Committee (IACUC) and followed officially approved procedures for the care and use of laboratory animals.

The livers were fixed in 10% paraformaldehyde and examined histologically. Histological slides were prepared by Patho-Lab Diagnostics Ltd., Ness Ziona, Israel. Paraffin-embedded tissues were sectioned at 5−6 μm and stained with Hematoxylin and Eosin (H&E). For the detection of IO nanoparticles, the tissues were stained with Prussian blue (PB). Stained slides were examined with an Olympus BX-51 microscope (Olympus, Melville, NY, USA). Any histopathological findings were recorded, described, and scored by a Board- certified study Pathologist, using semi-quantitative grading of five grades (0−4), taking into consideration the severity of the changes (0 = no lesion, 1 = minimal change, 2 = mild change, 3 = moderate change, 4 = marked change), as previously described.[4]

2.6. Cell Viability Assay. Cell viability was determined using a cell proliferation assay kit (cat no.: ab211091, Abcam, Cambridge, UK). Cells were seeded on 96-well plates at a density of 2.5×10^4 cells/well. After incubation for 24 h, the cell culture medium was replaced with 100 μL of fresh culture medium containing SaNPs (10−100 μg/mL). Following incubation for various time points (4, 24, and 48 h) at 37 °C, the cells were washed with PBS and assayed for cell viability. At each time point, the medium in the wells was replaced with 50 μL of serum-free culture medium without phenol red and 50 μL of 3-(4,5-dimethylthiazol-2-yl)-2,5-diphenyl tetrazolium bromide (MTT) reagent and incubated at 37 °C for 3 h. After incubation, the MTT reagent-supplemented media was removed, 150 μL of MTT solvent was added into each well, and the plates were incubated for 15 min at room temperature on an orbital shaker. The absorbance of the MTT-derived formazan was measured at 595 nm using a microplate reader (iMarkTM, BioRad Laboratories Inc., CA, USA). The percentage of cell viability was calculated using the following equation

$$\text{Percentage (\%) of cell viability} = (\text{sample OD}/\text{media control OD}) \times 100$$

The media control optical density (OD) represents the absorbance of cells without SaNP treatment.

2.7. Superoxide Dismutase Activity Assay. The activity of superoxide dismutase (SOD) was measured using a colorimetric activity assay kit as recommended by the manufacturer (cat. no.: ab65354, Abcam, Cambridge, UK). Briefly, the effect of SaNP on SOD activity was determined at time 0 and at 4, 24, and 48 h after incubation of 2×10^6 RAW264.7 cells with SaNP at two different concentrations of 10 μg/mL (low) and 100 μg/mL (high). Following incubation, the cells were harvested, lysed in ice cold 0.1 M Tris/HCl, pH 7.4 containing 0.5% Triton X-100, 5 mM β-ME, and 0.1 mg/mL PMSF, and centrifuged at 14,000*g* for 5 min at 4 °C. The supernatants containing the total SOD activity from both cytosolic and mitochondrial enzymes (MnSOD and CuZn-SOD) were collected. Unless analyzed immediately, the supernatants were stored in liquid nitrogen to preserve the enzymatic activity. The protein concentration in the samples was determined using Bradford reagent (cat. no.: ab119216, Abcam, Cambridge, UK) at 595 nm using BSA protein standards. The SOD assay was designed to quantitatively measure SOD activity. The absorbance values were recorded at 450 nm and the SOD activities of the samples were thereby calculated and normalized to the protein concentration present in the samples.

2.8. Measurement of Reactive Oxygen Species. Generation of reactive oxygen species (ROS) by RAW264.7

https://doi.org/10.1021/acsomega.4c07883
ACS Omega 2025, 10, 3535−3550

cells was quantitatively assessed using the cell-permeant 2′,7′-dichlorodihydrofluorescein diacetate (DCFDA)/H2DCFDA cellular ROS assay kit as recommended by the manufacturer (cat. no.: ab113851, Abcam, Cambridge, UK). DCFDA is a fluorogenic dye that measures ROS activity within live cells. It diffuses into cells and is then deacetylated by cellular esterases to a nonfluorescent compound, which is later oxidized in the presence of ROS into highly fluorescent 2′, 7′-dichlorofluorescein (DCF).[11]

RAW264.7 cells (2.5×10^3) were plated in a black flat-bottom 96-well plate and treated with SaNP at two different concentrations of 10 μg/mL (low) and 100 μg/mL (high) for 24 h. After incubation, the cells were washed, DCFHDA was added, and further incubated for 45 min at 37 °C. Fluorescence was measured using a hybrid multimode microplate reader (Synergy H1, BioTek, Fisher Scientific) at Ex/Em = 485/535 nm. *tert*-Butyl hydroperoxide (TBHP) solution (200 mM) was used as a positive control. For data analysis, blank readings were subtracted from all measurements and fold-change was determined between the control and treated samples.

2.9. TNF-α Release Assay. TNF-α levels were assayed in culture supernatants in duplicate by a colorimetric enzyme-linked immunosorbent assay (ELISA) kit for the quantitative detection of mouse TNF-α as per the manufacturer's instructions (cat. no.: BMS607-3, Invitrogen, USA). The effect of SaNPs on TNF-α production was determined after 4, 24, and 48 h of incubation of RAW264.7 cells (1×10^5 cells/well) with SaNP (10 μg/mL). Cell viability over 80% was observed for all SaNP treatments. For the assay, cell culture supernatants collected from SaNP-treated RAW264.7 cells were tested. Samples were aliquoted and stored frozen at 20 °C to avoid loss of bioactive mouse TNF-α. Prior to assay, the frozen samples were slowly brought to room temperature and gently mixed. A standard curve was created using known TNF-α concentrations between 31.3 and 2000 pg/mL. The absorbance of both the samples and standards was measured at 450 nm with a reference wavelength of 595 nm using an ELISA reader (iMarkTM, BioRad Laboratories Inc., CA, USA). The average absorbance values were calculated for each set of duplicate standards and samples and the concentration of circulating TNF-α for each sample was extrapolated from the standard curve.

2.10. Effect of Macrophage Conditioned Medium on Cancer Cell Growth and SaNP-Induced Cytokine Secretion. Conditioned medium (CM) was prepared by culturing RAW264.7 cells in the presence of SaNPs (100 μg/mL) for 24 h at 37 °C. CM from untreated RAW264.7 cells served as a control. The medium of treated and untreated cells was harvested and centrifuged at 7,000*g* for 2 h at 4 °C to remove cell debris and SaNPs. The cleared CM was then added to 4T1 TNBC cells at two different densities (2.5×10^5 and 5×10^5 cells/mL) cultured on a flat-bottom 96-well plate and incubated for an additional 24 h. Cell viability was determined by an MTT assay as described above. Cytokine expression in CM was examined using a proteome profiler (Mouse cytokine array panel A, cat. no.: ARY006, R&D SystemsTM, Boston, USA) intended for the parallel determination of the relative levels of selected mouse cytokines and chemokines, as recommended by the manufacturer, using chemiluminescence. Positive signals were identified, and pixel densities were analyzed. The average signal of the pair of duplicate spots representing each cytokine was calculated by subtracting an average background signal from each spot and comparing the corresponding signals on different arrays (control vs treatment) to determine the relative change in cytokine levels between samples.

2.11. Confocal Microscopy. The cellular internalization and localization of SaNPs in mCherry-4T1 and RAW264.7 macrophage cells were investigated by incubating the cells with FITC-labeled SaNPs for 24 h at 37 °C in a humidified incubator with 5% CO_2. Confocal microscopy was conducted by staining RAW264.7 cells with the lysosomal CytoPainter staining kit (cat. no.: ab112137, Abcam, Cambridge, UK), and DAPI for nuclear staining. RAW264.7 cells grown in standard DMEM medium were washed with PBS, followed by scraping. The cell suspension was centrifuged at 125*g* for 10 min and resuspended in fresh medium for counting. On day 1, the cells were counted, diluted with culture medium, and seeded on glass coverslips in a 6-well plate at a density of 1.5×10^5 cells/mL. One day after seeding, the cells were incubated at 37 °C without (control) or with FITC-labeled SaNP at a 1:20 dilution (50 μg/mL), for 24 h. Each treatment was carried out in triplicates. Following incubation with FITC-labeled SaNPs (day 2), the cells were gently washed thrice with PBS in the dark. For the staining, a dye working solution was prepared by diluting 20 μL of dye stock solution in 10 mL of live cell staining buffer. One mL of staining solution was added to each plate and the cells were incubated in a 37 °C, 5% CO_2 incubator for 1−2 h and then washed twice with prewarmed PBS, in the dark. Following washes, RAW264.7 cells were fixed in 4% buffered PFA solution for 15 min. The cells were washed thrice in PBS, and then permeabilized by incubation with 0.1% Triton X-100 solution in PBS for 10 min and further washed in PBS for 5 min. A DAPI stock solution of 5 mg/mL (14.3 mM) was prepared, and the cells were stained with a final 300 nM DAPI stain solution using a standard procedure. Following permeabilization, the cells were washed thrice in PBS. Sufficient DAPI stain solution was added to cover the cells and incubated for 1−5 min, protected from light. The stain solution was removed, and the cells were washed thrice in PBS. The coverslips were mounted using Fluoroshield mounting media and stored in the dark at 4 °C until analysis. Imaging was performed using a Leica STED scanning confocal microscope using a 63×/1.40 OIL objective. The stained lysosomes were visualized with excitation of a 552 nm laser and emission between 569 and 640 nm. Data acquisition was performed using the Leica Application Suite X (LASX) software (Leica Microsystems, Mannheim, Germany).

2.12. Prussian Blue Staining. RAW264.7 cells grown in standard DMEM medium were washed with PBS, followed by scraping. The cell suspension was centrifuged at 370*g* for 5 min and resuspended in fresh medium for counting. On day 0, the cells were counted, diluted with culture medium, and seeded on glass coverslips in 6-well plates at a density of 1.5×10^5 cells/mL. Four hours after seeding, the cells were incubated without (control) or with FITC-labeled SaNP for 24 h at 37 °C in a humidified incubator with 5% CO_2. Following incubation, the cells were gently washed thrice with PBS in the dark and fixed as described above. Prussian blue stain solution (cat. no.: ab150674, Abcam, Cambridge, UK) was prepared by mixing equal amounts of potassium ferrocyanide solution and hydrochloric acid solution to make a working iron stain solution. All materials were equilibrated at room temperature before use. The coverslips were then incubated in working iron stain solution (2−3 mL/plate) for 3 min,

https://doi.org/10.1021/acsomega.4c07883
ACS Omega 2025, 10, 3535−3550

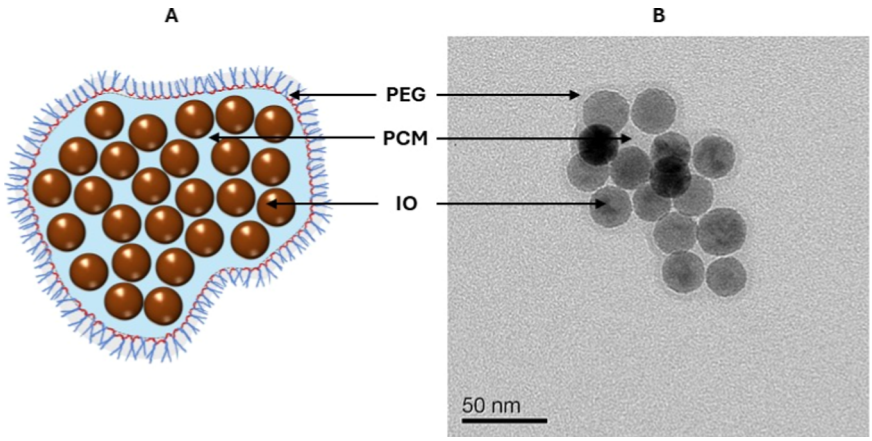

Figure 1. Physicochemical characteristics of SaNP. (A) Schematic illustration of a multicore SaNP containing PEG 20,000-encapsulated IO nanoclusters and a PCM core. (B) Representative TEM image of SaNP. A scale bar is indicated. Images were obtained using a Tecnai G2Spirit Twin T-12 electron microscope with an accelerating voltage of 120 kV.

followed by extensive rinsing with double distilled water (DDW). The cells' nuclei were counterstained in nuclear fast red solution for 5 min and further rinsed 4 times with DDW. A dehydration step was carried out in 95% alcohol followed by absolute alcohol and the slides were then cleared and mounted using Fluoroshield mounting media. The stained slides were stored at 4 °C to prevent desiccation. Imaging was performed using a Leica upright DM6Z wide-field microscope using a 63× magnification. Data acquisition was performed using the Leica Application Suite X (LASX) software (Leica Microsystems, Mannheim, Germany).

2.13. Transmission Electron Microscopy. RAW264.7 cells were seeded and incubated on 10 cm culture plates at a density of 3×10^6 cells per plate for 24 h before the experiment. The cells were then treated with SaNPs at a 1:100 dilution (10 μg/mL) in serum-free media. The control cells were treated with medium alone. Following SaNP treatment, the SaNP-containing media was removed, and the cells were thoroughly washed thrice with PBS. The cells were then fixed for 2 h in Karnovsky fixative (2.5% glutaraldehyde with 2.5% paraformaldehyde) in 0.1 M sodium cacodylate buffer (pH 7.4) and washed with the same buffer. The cells were postfixed in 1% OsO_4, in 0.1 M cacodylate buffer (pH 7.4) for 1 h at room temperature, then washed twice with 0.1 M cacodylate buffer, followed by rinsing with DDW three times. Cells were then stained with 2% uranyl acetate for 1 h, washed with DDW, dehydrated in ethanol, and embedded in Epon Embed 812 (EMS, PA, USA). The resin was polymerized at 60 °C for 24 h. Ultrathin sections (70−90 nm) were obtained with a Leica ultracat (UC7) ultramicrotome (Leica Microsystems, Mannheim, Germany). The samples where then examined with a Tecnai G2 G2Spirit Twin T-12 electron microscope (FEI—Teramo Fisher) with an acceleration voltage of 120 kV (Bar Ilan University, Israel). Images were taken using a digital micrograph with a multiscan camera model 794 (Gatan) at different resolutions.

2.14. Imaging Flow Cytometry. RAW264.7 cells were seeded at a density of 3×10^5 in 10 cm plates in standard DMEM medium and incubated for 24 h. Then the culture medium was replaced with fresh medium with or without FITC-labeled SaNP (1.83 mg/mL) at a 1:20 dilution (50 μg/mL), and the cells were reincubated for additional 24 h after which the medium was removed, the cells were rinsed twice with PBS to eliminate free FITC-SaNPs not taken up by the cells, and fresh culture medium was added to the plates. This time point was considered as day 0. The cells were then incubated and cultured for 1−3 days. Cells incubated with medium without SaNPs were used as a control for each time point. Each sample was prepared by scraping, counting the cells, and bringing to a density of 1×10^6 cells/sample in 1.5 mL Eppendorf tubes for measurement. The FITC-SaNP uptake by the cells was quantified using multispectral imaging flow cytometry (ImageStream markII flow cytometer). Samples were run in the ImageStream and imagery was acquired for 5000 events in each sample using the 60× objective. Mean intensity of FITC-SaNP (channel 2, Ex/Em = 488/480−560 nm) was calculated.

2.15. Examination of SaNP Enzymatic Degradation. To investigate the potential enzymatic degradation of SaNPs, various enzymes such as FBS, trypsin, and AST were used.[12]

SaNPs at a defined concentration of 1 mg/mL were incubated with FBS (1%), trypsin (0.01%), or AST (5 U/L) at a 1:1 dilution for 24 h in sterile glass vials at 37 °C in a biological incubator. SaNPs dispersed in WFI and incubated at 37 °C for 24 h were used as a control for the stability of the nanoparticles, under the same testing conditions at neutral pH. The vials were inverted several times and mixed throughout the incubation period. Following incubation, the samples were recovered by centrifugation at 5000*g* at 4 °C for 60 min. The pellets were reconstituted in WFI and sonicated for 6 min at room temperature. SaNP characteristics in samples (0.2 mL) were measured before and after incubation by DLS analysis using a Zetasizer nano-ZS (Malvern Panalytical, Malvern, UK) to determine changes in physicochemical properties including hydrodynamic size and zeta potential.

2.16. Statistical Analysis. All values were expressed as mean ± standard deviation (SD). The statistical significance of differences between groups was analyzed by Student's *t*-test and a *p*-value of <0.05 was considered as statistically significant. Comparison of results among groups was carried out by one-way analysis of variance (ANOVA). Data were organized using Microsoft Excel (Microsoft Corporation, Redmond, WA, USA) and statistical calculations were carried out using GraphPad Prism v.9.4.1 (GraphPad Software, Inc., San Diego, CA, USA).

https://doi.org/10.1021/acsomega.4c07883
ACS Omega 2025, 10, 3535−3550

3. RESULTS

3.1. Physicochemical Characterization of SaNPs. The physicochemical characteristics of SaNPs were determined by DLS and TEM. TEM imaging demonstrated that SaNPs, containing several encapsulated 25 ± 2 nm IO nanoparticles, exhibit a monodisperse state and amorphous or nonspherical shapes, which provide the nanoparticles with their flexibility features (Figure 1). DLS results showed an average size of 123.9 ± 2.592 nm and an average zeta potential of (−16.5) ± 0.153 mV. SaNP specifications are summarized in Table 1.

Table 1. SaNP Specifications[a]

attribute	specification
size	90−165 nm
surface charge/zeta potential	(−5)−(−30) mV
appearance	brown dispersion without aggregates
concentration	1,4−4.2 mg/mL
morphology	amorphous and non-spherical shape with rigid 25 nm IO magnetite encapsulated nanoparticles

[a]Size (diameter) and zeta potential (mV) values were determined by DLS.

3.2. In Vitro Cytotoxicity of SaNPs. Previous studies conducted in both porcine proximal tubule kidney LLC-PK1 and human hepatocarcinoma HepG2 cells, according to ASTM E2526-08 (2013): guideline for standard test method for evaluation of cytotoxicity of nanoparticulate materials, using SaNPs at various dilutions with a broad concentration range and two different evaluation methods, MTT and LDH assays, demonstrated that SaNPs were noncytotoxic, showing high viability (>70%), low LDH release (<30.5%) in both cell lines, and met the guideline accepting criteria thus supporting their safety (unpublished data).

To investigate whether SaNPs can exert direct cytotoxic effects on macrophages, RAW264.7 cells were grown in the presence of SaNPs at different concentrations of 0−100 μg/mL for various time points of 4, 24, and 48 h. Following treatment, the percentage of cell viability was determined by an MTT assay. The results indicated that SaNPs effects on macrophage cell viability were both time- and concentration-dependent. Reduced cell viability was observed at the higher SaNP concentrations (50−100 μg/mL) whereas lower concentrations (10 μg/mL) had a lesser impact, depending on the time of exposure (Figure 2).

3.3. SaNP-Induced SOD Activation and ROS Generation. Reactive oxygen species (ROS) play important roles in the modulation of cell signaling involved in cell death, proliferation, and differentiation. Following the uptake of SaNPs by macrophages, ROS can be potentially generated. Activation of the NADPH oxidase pathway due to SaNP uptake, can be examined by measuring the activity of several enzymes including NADPH oxidase (NOX), superoxide dismutase (SOD), and myeloperoxidase (MPO). SOD activation forms the front line of defense against oxidative stress in the body, plays a major role in regulating the intracellular concentration of superoxide and protecting cells from its harmful effects by converting two superoxide anions to oxygen and hydrogen peroxide (H_2O_2). Then, MPO catalyzes oxidation of chlorides to high bactericidal hypochlorites with the participation of H_2O_2.[8]

In this study, the activity of SOD was measured in cell lysates using a colorimetric activity assay. SOD enzymes are expressed in different cellular compartments. For example, manganese-containing SOD (MnSOD) is localized in the mitochondria while copper- and zinc-containing SOD (CuZnSOD) is mostly cytoplasmic. The cell lysate supernatants contained both isozyme forms. The effect of SaNP on SOD activity was determined at time 0 and 4, 24, and 48 h after incubation of RAW264.7 cells with SaNP at two different concentrations of 10 μg/mL (low) and 100 μg/mL (high) (Figure 3A). The results demonstrated that in RAW264.7 cells treated with a low concentration of SaNP (10 μg/mL), SOD activity was reduced compared to the untreated control suggesting that no superoxide was generated at the tested time points and therefore, the enzyme was not activated by SaNPs' presence. The percentage of SOD activity at time 0 represents the baseline activity in the cells under the conditions of the study. On the other hand, in cells incubated with a higher SaNP concentration (100 μg/mL), the percentage of SOD activity at 4 and 24 h after SaNP treatment was elevated compared to the control, indicating enzyme activation due to ROS generation at these time points. The differences between the time points were statistically significant as demonstrated by one-way ANOVA. No activity was detected after 48 h of SaNP treatment at the higher concentration, probably because the activation of SOD eliminated SaNP-induced ROS from the

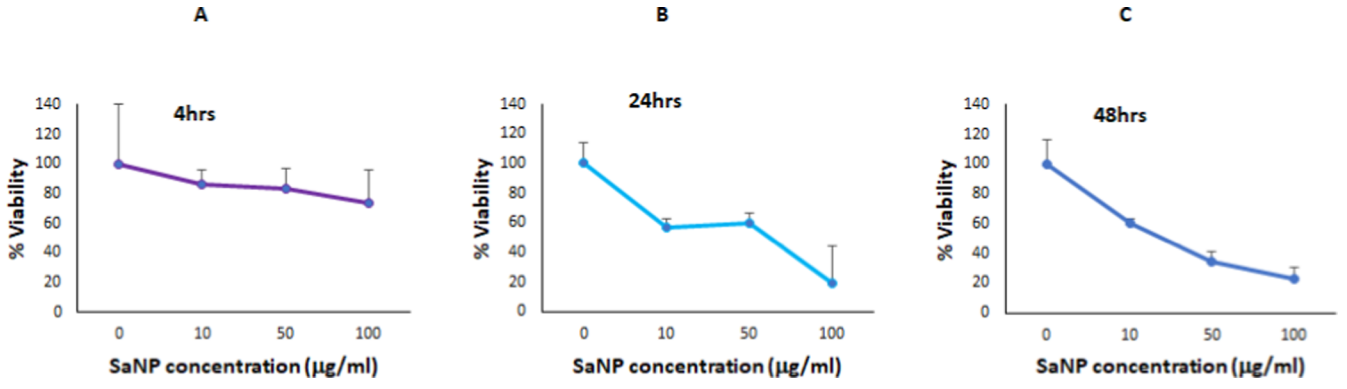

Figure 2. Effect of SaNPs on macrophage cell viability. RAW264.7 cells were treated with SaNPs at different concentrations (0−100 μg/mL) for various time points of; (A) 4, (B) 24, and (C) 48 h. Cell viability was determined by an MTT assay. Results are representative of 3 independent experiments.

https://doi.org/10.1021/acsomega.4c07883
ACS Omega 2025, 10, 3535−3550

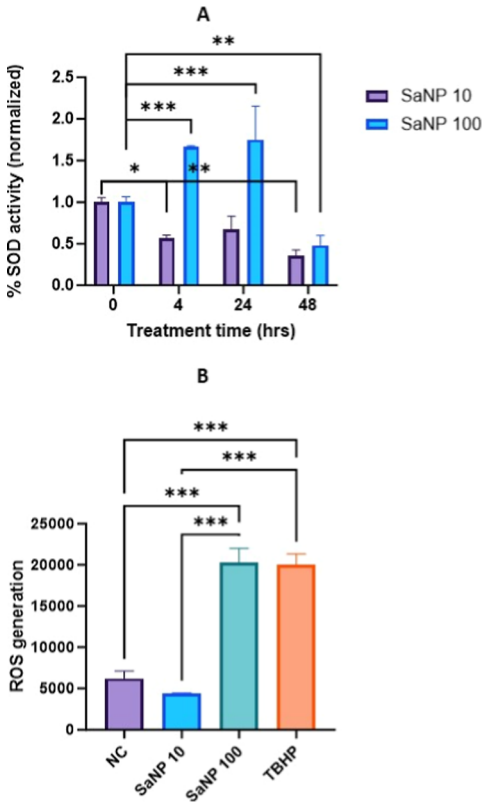

Figure 3. SaNPs affect the activity of SOD and induce ROS generation. (A) RAW264.7 cells were incubated with SaNPs at a low (10 μg/mL) and high concentration (100 μg/mL) for 0, 4, 24, and 48 h. Following treatment, cell lysates were prepared and assayed for SOD activity. (B) ROS generation was measured in live cells using the DCFDA/H2DCFDA method. RAW264.7 cells were treated with SaNP concentrations of 10 μg/mL (low) and 100 μg/mL (high) for 24 h. *tert*-Butyl hydroperoxide (TBHP) was used as positive control. Untreated cells served as a negative control (NC). The results are representative of 3 different experiments. *p-value < 0.05; **p-value < 0.001; ***p-value < 0.0001.

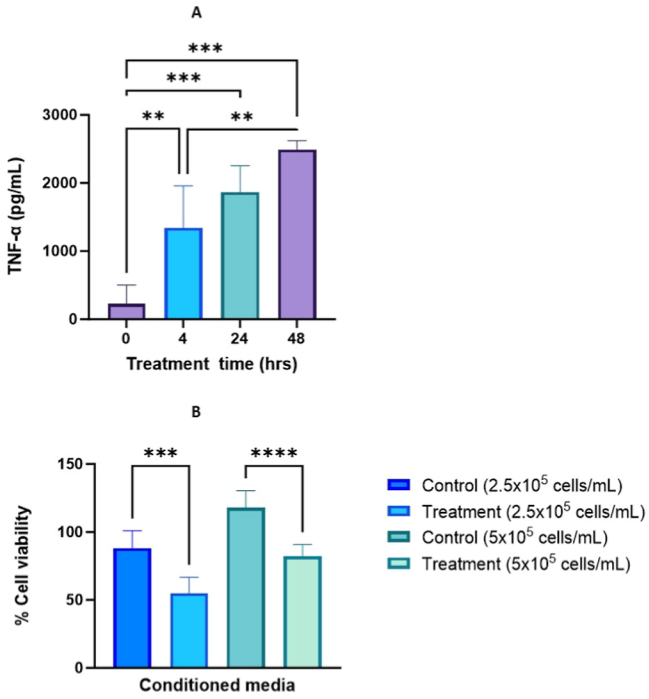

Figure 4. SaNPs induce TNF-α release by macrophage cells and macrophage-conditioned medium (CM) inhibit cancer cell viability. (A) TNF-α release by SaNP-treated (10 μg/mL) RAW264.7 cells was examined at various time points. Supernatants were collected after 0 (control), 4, 24, and 48 h of treatment and assayed for TNF-α levels by ELISA. Absorbance was read at 450 nm (595 nm as reference wavelength). (B) The effect of CM on the cell viability of cancer cells was determined by an MTT assay. CM was prepared by incubating RAW264.7 cells with or without SaNPs (100 μg/mL) for 24 h and added to 4T1 TNBC cells (either 2.5×10^5 or 5×10^5 cells/mL) for an additional 24 h. **p-value < 0.001; ***p-value < 0.0001. The results are representative of 3 independent experiments.

system, and the activity was similar to that induced at the low concentration.

ROS generation was also directly measured after treatment of RAW264.7 cells with either low or high SaNP concentrations (10 or 100 μg/mL, respectively) for 24 h, the time point at which the highest SOD levels were detected. The results demonstrated that ROS levels were not affected by low SaNP but significantly increased in the presence of high SaNP at a level comparable to that of the positive control (TBHP), compared to the untreated negative control (NC) cells (Figure 3B).

3.4. SaNP-Induced Production of Cytokines in Macrophage Cells and Inhibition of Cancer Cell Growth by Macrophage-Conditioned Medium. TNF-α is a multifunctional cytokine involved in several different pathways, playing an important role in various cellular processes such as apoptosis, cell survival, inflammation, and immunity. TNF-α is secreted by activated monocytes and macrophages, and other cells, including B cells, T cells and fibroblasts. It is a major pro-inflammatory cytokine that is expressed in the early stage of cell inflammation and induces apoptosis by several known pathways.[13] The effect of SaNP (10 μg/mL) on TNF-α release was determined after 0 (control group without SaNP), 4, 24, and 48 h of incubation with RAW264.7 cells (Figure 4A). The amount of TNF-α at time 0 represents the baseline activity in the cells under the conditions of the study. Cell viability over 80% was observed for all SaNP treatments. The results showed that TNF-α release by RAW264.7 cells treated with SaNPs increased with time, suggesting that SaNPs induced activation of the macrophage cells which in turn released TNF-α into the growth medium and in correlation with the decrease in cell viability (~20%). A statistically significant difference was found between the control and all other time points (one-way ANOVA, ***p-value < 0.0001) and between the time points of 4 and 48 h (one-way ANOVA, **p-value < 0.001).

One of the main features of macrophages is their high plasticity, which allows them to respond to stimuli from the complex tissue microenvironment, by rapidly changing their functional profile through a process termed polarization.[14] Macrophages can be characterized as being activated into two main classes, M1 and M2. M1 macrophages are associated with inflammation, including secretion of pro-inflammatory cytokines, engulfment of foreign entities, generation of ROS, and initiation of immune responses. Conversely, M2 macrophages perform anti-inflammatory and wound repair functions. In general, M1/M2 phenotypes describe two major and opposing activities of macrophages. M1 activity inhibits cell proliferation and causes tissue damage while M2 activity promotes cell proliferation and tissue repair. The tumor microenvironment can release factors that drive macrophages toward an M2-like phenotype, resulting in secretion of anti-inflammatory

https://doi.org/10.1021/acsomega.4c07883
ACS Omega 2025, 10, 3535−3550

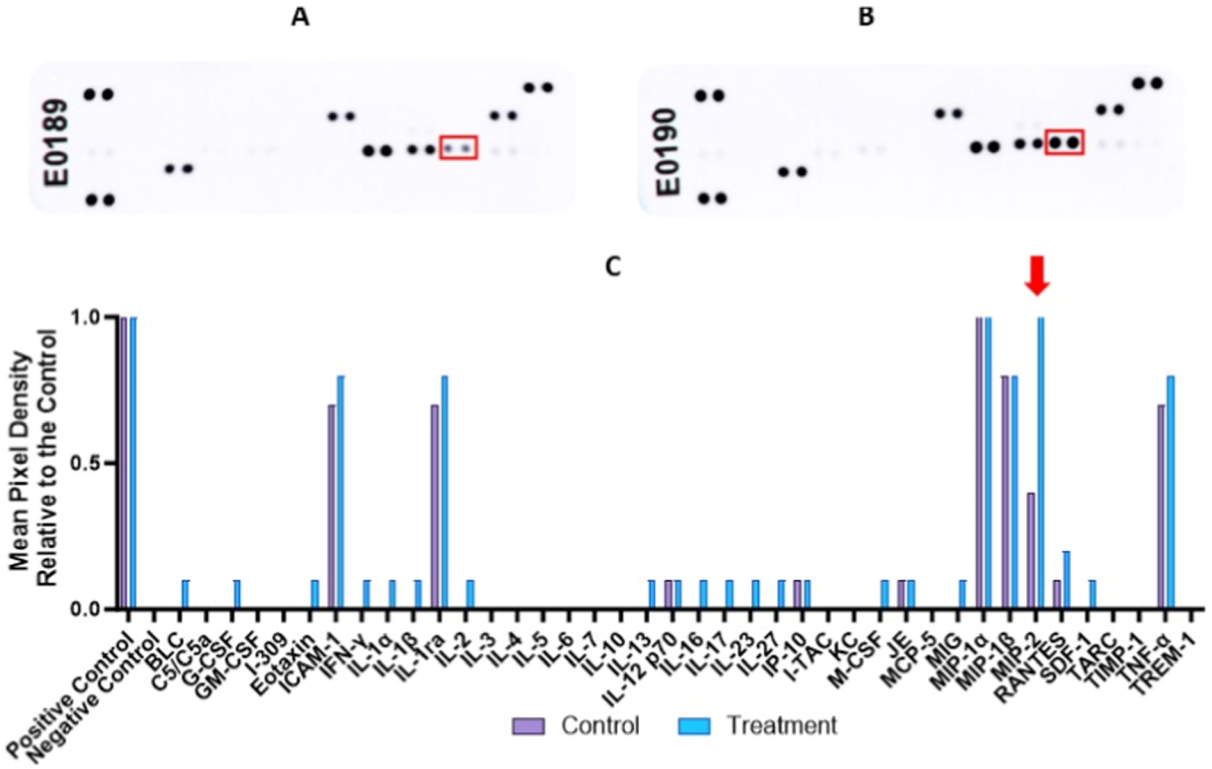

Figure 5. Relative expression of cytokines in CM from SaNP-treated macrophage cells. (A) CM was prepared from either untreated (control) RAW264.7 cells or (B) cells treated with SaNPs (100 μg/mL) for 24 h. (C) Cytokine expression in CM was determined, positive signals were identified, and mean pixel densities relative to control were calculated and compared. Red squares denote the main difference in control vs treatment.

cytokines, promotion of tumor growth, invasion, and facilitation of metastases.[15]

The role of different nanoparticles in macrophage cellular activation and the promotion of a specific phenotype is not well-defined. Therefore, we sought to examine the effect of conditioned medium (CM) from SaNP-treated RAW264.7 cells compared to CM from untreated macrophages (control) on the proliferation of murine 4T1 triple negative breast cancer (TNBC) cells used as a metastatic cancer model.[4] The effect of CM on cancer cell viability was measured by an MTT assay at two different cell densities (2.5 and 5 × 10^5 cells/mL). In both cases, the results showed that CM from SaNP-activated macrophages inhibited 4T1 cell proliferation compared to the control suggesting an antitumor effect driven by SaNPs and supporting a classically activated M1 phenotype (Figure 4B). However, further analysis with specific markers is required to characterize this macrophage phenotype.

To understand the potential role of macrophage-secreted factors in the inhibition of 4T1 cancer cell proliferation, a cytokine array panel was used (Figure 5). CM was prepared as described above, from SaNP-treated and untreated (control) macrophage cells, and then assayed on two separate arrays to simultaneously detect differences between the samples. The relative expression of 40 mouse cytokines was measured and average signals (e.g., mean pixel densities) were calculated and compared to those of the control. As demonstrated by the results, differences were detected between the arrays. A significant change was observed in the relative expression of macrophage inflammatory protein-2 (MIP-2) in the CM of SaNP-treated cells (Figure 5B, red arrow) compared to that of untreated cells. In addition, increased levels of interleukin-1 receptor antagonist (IL-1Ra), an anti-inflammatory antagonist of the interleukin-1 family of pro-inflammatory cytokines, intercellular adhesion molecule 1 (ICAM-1), and RANTES were also observed but to a lesser extent. Notably, increased levels of TNF-α were detected in the CM of SaNP-treated macrophages, supporting our previous data (Figure 4A).

3.5. SaNP Internalization and Intracellular Localization in Macrophage Cells. The localization of FITC-labeled SaNPs was first evaluated in mCherry-4T1 TNBC cells. Cells were incubated with FITC-SaNP at various dilutions of 1:10, 1:20, and 1:200 (corresponding to 100, 50, and 5 μg/mL, respectively) for 24 h. Untreated cells served as a negative control whereas cells treated with unlabeled SaNP served as a positive control. The results demonstrated that SaNPs rapidly internalize, localize, and accumulate within the cell cytosol of the malignant cells. The higher concentrations of 100 and 50 μg/mL rendered similar results, whereas at 5 μg/mL the green fluorescence was barely visible. Thus, the FITC fluorescence decreased with decreasing FITC-SaNP concentrations, demonstrating reduced cellular uptake at lower concentrations. No green fluorescence was observed in the cytoplasm of the untreated control 4T1 cells (data not shown). Representative images obtained in cells treated with 50 μg/mL FITC-SaNP are presented (Figure 6).

The cellular internalization and localization of SaNPs in RAW264.7 macrophage cells were examined by confocal microscopy following incubation with FITC-labeled SaNPs for 24 h at the selected dilution of 1:20 (50 μg/mL). SaNP localization was examined by triple staining of cells with CytoPainter, a hydrophobic lysotropic dye that serves as an

https://doi.org/10.1021/acsomega.4c07883
ACS Omega 2025, 10, 3535−3550

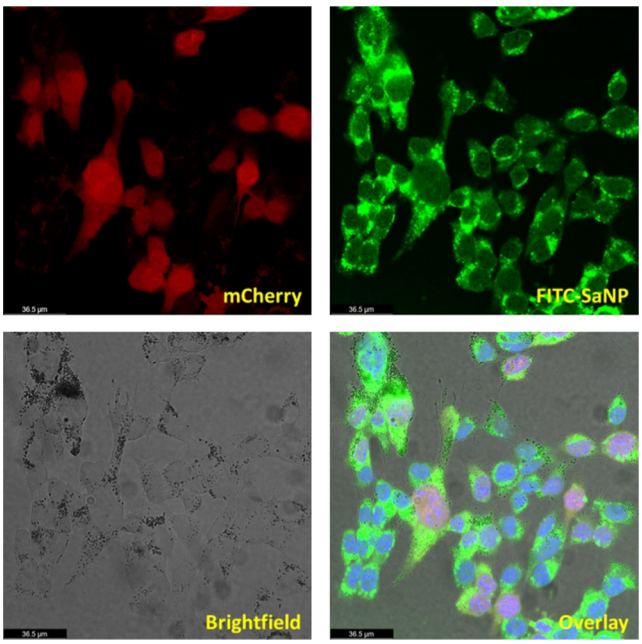

Figure 6. Internalization and intracellular localization of FITC-SaNP in mCherry-4T1 TNBC cells. mCherry expressing 4T1 cells were treated with FITC-SaNP at a 1:20 dilution (50 μg/mL) and counterstained with DAPI. Cells were visualized with a Leica TCS SP8 STED confocal system using a 63× magnification. Brightfield microscopy image of 4T1 cells is also shown. Scale bars are indicated.

imaging tool for labeling subcellular organelles, and DAPI for nuclear staining.

Lysosomes are cellular organelles that contain acid hydrolytic enzymes to break up waste materials and cellular debris, are composed of an acid lumen and a layer of lysosomal membrane formed by a phospholipid bilayer which allows the digestive enzymes to work at an acidic pH of 4.5. They digest excess or worn-out organelles, particles, and engulfed viruses or bacteria and play key roles in degradation, innate and adaptive immunity, and nutrient sensing.[16] CytoPainter (Ex/Em = 575/600 nm) permeates intact live cells and selectively accumulates in lysosomes, probably through the lysosome pH gradient. Its fluorescence is strongly enhanced upon entering lysosomes and is specific to lysosomes.[17] The results indicated that FITC-SaNPs were up taken by the macrophage cells and specifically colocalized within the lysosomal compartment, as indicated by the specific staining (Figure 7A). The colocalization of SaNPs and lysosomes showed up as yellow fluorescence in the overlay between green fluorescence nanoparticles and red fluorescent-vesicles. A large number of nanoparticles were observed inside the vesicles, suggesting their rapid entrance and internalization to the cell cytoplasm.

To further confirm the specific localization of FITC-SaNP in lysosomes and its potential cellular degradation, RAW264.7 macrophage cells were stained with Prussian blue which detects the presence of ferric iron in tissues and cells and is based on the chemical reaction of ionic iron with acid ferrocyanide to produce a blue color (Figure 7B). Nuclear fast red was used for counterstaining. The results further confirmed that FITC-SaNP undergo internalization in RAW264.7 macrophage cells and generate a strong Prussian blue stain cytosolic reaction, with many blue particles in the cytoplasm of RAW264.7 cells, due to the presence of IO containing SaNPs in this compartment. In contrast, no blue particles were detected in the negative control untreated cells (data not shown). Of note, nonphagocyted SaNPs were observed on the background of the imaged plane and were stained by Prussian blue; these SaNPs remained intact and resembled those engulfed by the cells.

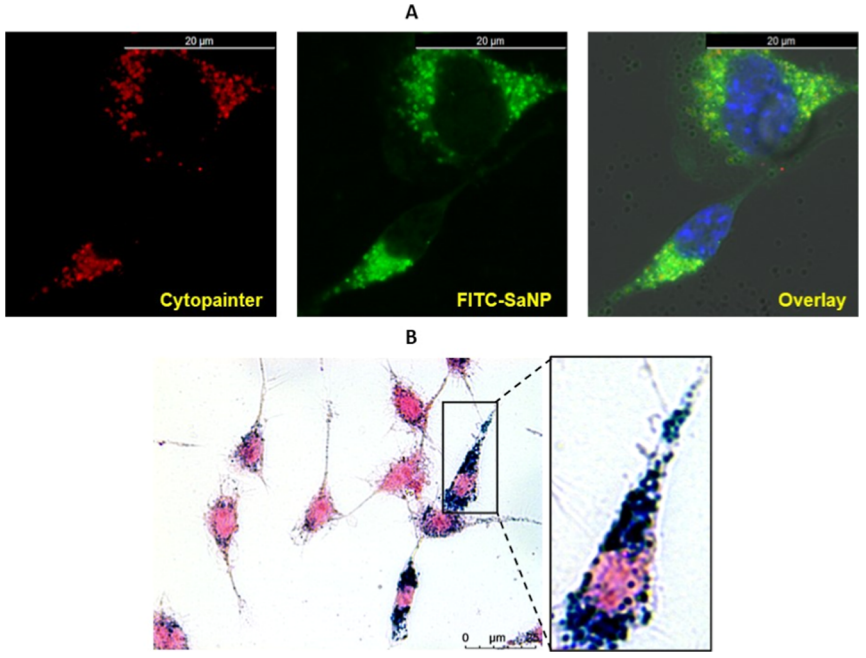

Figure 7. FITC-SaNPs colocalize within lysosomes of macrophage cells. (A) RAW264.7 cells were incubated with FITC-SaNP diluted 1:20 (50 μg/mL) for 24 h. Images were visualized using a 63× magnification and a ×2.35 zoom (Leica TCS SP8 STED confocal system). (B) Prussian blue and nuclear fast red counterstaining of RAW264.7 cells treated with FITC-SaNP for 24 h (Leica Microsystem LMD7, 63× magnification). Scale bars are indicated. Results are representative of 3 independent experiments.

https://doi.org/10.1021/acsomega.4c07883
ACS Omega 2025, 10, 3535−3550

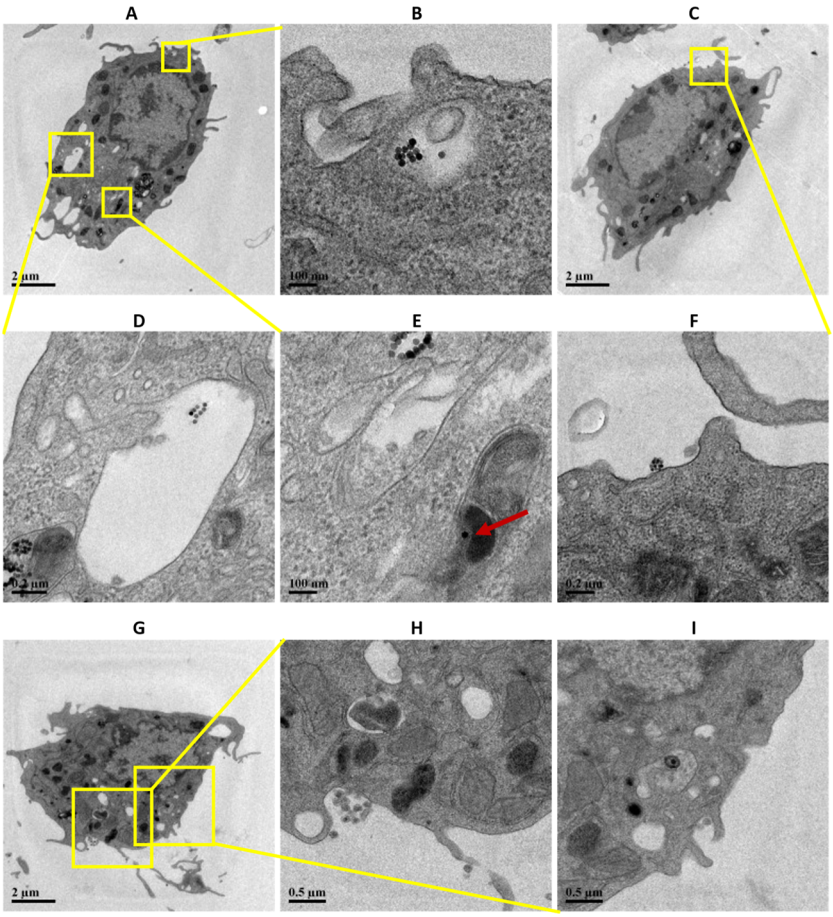

Figure 8. Transmission electron microscopy (TEM) examination of morphological changes in RAW264.7 cells following SaNP uptake and subcellular distribution. (A–F) TEM images of macrophages were taken after SaNP treatment (10 μg/mL) for 24 h. SaNPs were captured inside the lysosomes, maintaining their psychochemical characteristics in terms of size and shape. (E) SaNP in mitochondria (red arrow). (F) Macrophage pseudopodia engulfing SaNPs. (G–I) Untreated control cell. Images were taken using a digital micrograph with a multi-scan camera model 794 (Gatan) at different resolutions. Scale bars are indicated.

To detect morphological changes and potential degradation of the internalized SaNPs within the lysosomes of engulfing macrophages, RAW264.7 cells were treated with SaNPs for 24 h in serum-free media and observed under TEM to determine their distribution in the subcellular structures (Figure 8). As demonstrated by the results, following treatment with SaNPs, numerous nanoparticles were clearly observed in the cytoplasm of the treated cells, that localized both in endosomal vesicles and lysosomes (Figure 8A–F). The SaNPs were mostly inside vacuoles dispersed throughout the cytosol. No nanoparticles were found in the cytosol of untreated cells (Figure 8G–I). Interestingly, SaNPs were also observed in the mitochondria (Figure 8E). The shape of the SaNPs remained amorphous but mostly intact, suggesting that the nanoparticles did not undergo degradation. TEM imaging was able to capture macrophages with several pseudopodia, required for motility and ingestion, actively engulfing SaNPs. Nevertheless, the cellular morphology was not affected by the treatment, which is consistent with the MTT cell viability assay results (Figure 2) at the tested concentration (10 μg/mL).

3.6. SaNPs are Cleared from Macrophage Cells Over Time. Previous animal studies have shown that SaNPs are cleared from the body within the first days after treatment.[6] To monitor changes in the intracellular quantities of SaNPs over time after uptake by macrophages, a high-throughput imaging flow cytometry method was used for simultaneous analysis of multiple images obtained from brightfield and fluorescence channels combined with flow cytometry data. The system gathers image capture with image quantification and enables discrimination of cells based on their morphology.[18]

RAW264.7 cells were treated with FITC-labeled SaNP at a 1:20 dilution (50 μg/mL) for 24 h, after which the medium was removed, and the cells were washed to eliminate free FITC-SaNPs not taken up by the cells. This time point was considered as day 0. The cells were then additionally cultured for days 1 and 3. For each time point, the FITC-SaNP fluorescence intensity signals were compared to the initial signals obtained on day 0. Cells incubated in medium without FITC-SaNPs (unstained) were used as controls for each time point. FITC and brightfield images were visualized (Figure 9). The mean intensity of the FITC-SaNP was measured and calculated. A significant reduction of 64.3% in the mean signal intensity of FITC-SaNP was found on day 1 compared to day 0, and a similar reduction of 66.4% in the mean signal intensity was found on day 3 compared to day 0. The reduction in the signal intensities compared to day 0 suggests that SaNPs are cleared from the macrophage cells over time within this time frame. The differences were statistically significant (p-value < 0.0001, one-way ANOVA). The morphology of the cells remained unaltered at days 0 and 1, similar to the TEM results,

https://doi.org/10.1021/acsomega.4c07883
ACS Omega 2025, 10, 3535–3550

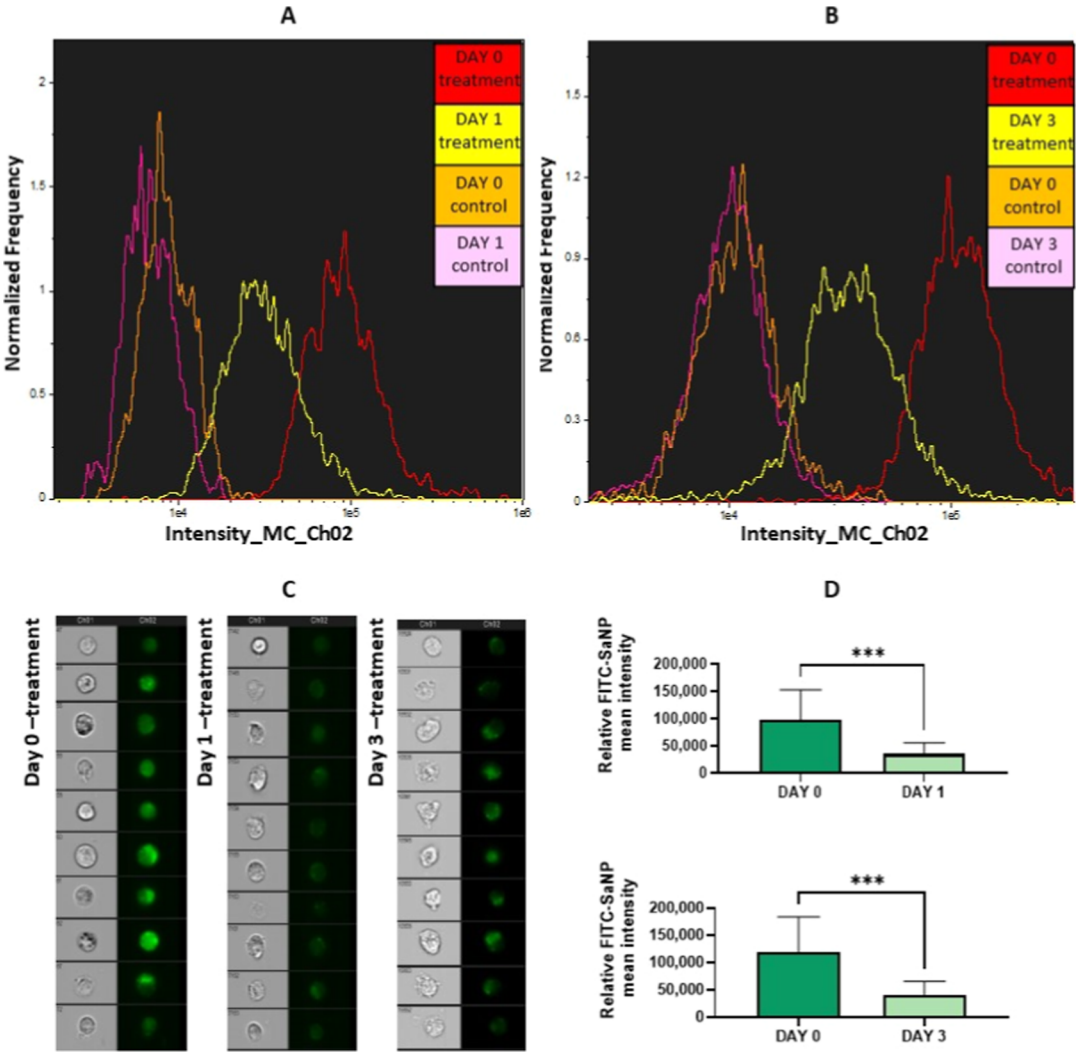

Figure 9. Clearance of FITC-SaNPs from macrophage cells over time. FITC-SaNP treated RAW264.7 cells were analyzed by imaging flow cytometry on days 0, 1, and 3 after treatment. (A,B) Normalized frequency of the signal intensities of FITC-SaNPs measured after treatment on days 0 and 1 or days 0 and 3. The cell counts, mean signal intensities and standard deviations were calculated. (C) Representative images of collected cells captured by imaging flow cytometry on the brightfield and FITC channels. (D) Relative mean intensity of FITC-SaNP signals on days 0 vs day 1 and day 0 vs day 3. ***$p < 0.0001$.

but changes were observed on day 3, probably reflecting the clearance process.

3.7. Histological Examination of SaNP Accumulation in the Liver. The results of the histological analysis on day 3 after SaNP administration demonstrated no treatment-related changes in the liver (Figure 10). Minimal pigment laden macrophages (i.e., Kupffer cells), associated with minimal inflammatory mononuclear cell infiltration were observed in the liver of 3 out of 5 treated mice and scored by the study pathologist as grade 1. A similar inflammatory cell infiltration was observed in one out of 5 mice in the control group. As the changes in the liver were of minimal degree, were not found to be associated with any potential degradation, they were not considered as adverse according to the criteria of the Society of Toxicologic Pathology (STP)[19] and SaNPs were deemed safe for use, as supported by previous studies.[4]

3.8. SaNPs Do Not Undergo Enzymatic Degradation. Following in vitro or in vivo administration, nanoparticles may be exposed to different local environments during their uptake. Thus, intravenous injected SaNPs would first travel through the circulation followed by internalization to the acidic endosomes/lysosomes of macrophages. Upon cellular uptake and internalization, potential enzymatic degradation of SaNPs may occur. Proteolytic enzymes present in endosomes or lysosomes can digest amphiphilic polymer coatings based on amide bonds. The coating of inorganic nanoparticles, such as PEG-containing IO nanoparticles can also be degraded in lysosomes by other intracellular enzymes which may affect their physicochemical properties and thus, their fate.

To examine potential degradation after exposure to various enzymes using a non-cellular method, SaNPs were incubated with FBS, trypsin, or AST for 24 h. FBS, which resembles human serum, was used to evaluate the degradation of SaNPs by enzymes present in the blood. Trypsin, a serine protease, is an important digestive enzyme broadly expressed in normal tissues, secreted by the pancreas but also expressed in other tissues including the kidney, liver, lungs as well as splenic and neuronal cells. Trypsin has a potent proteolytic activity and was shown to cleave the C-terminal of arginine and lysine residues which are then converted to amino acid derivatives.[20] AST is an important enzyme in the amino acid metabolism that catalyzes the reversible transfer of amino acid groups and

https://doi.org/10.1021/acsomega.4c07883
ACS Omega 2025, 10, 3535−3550

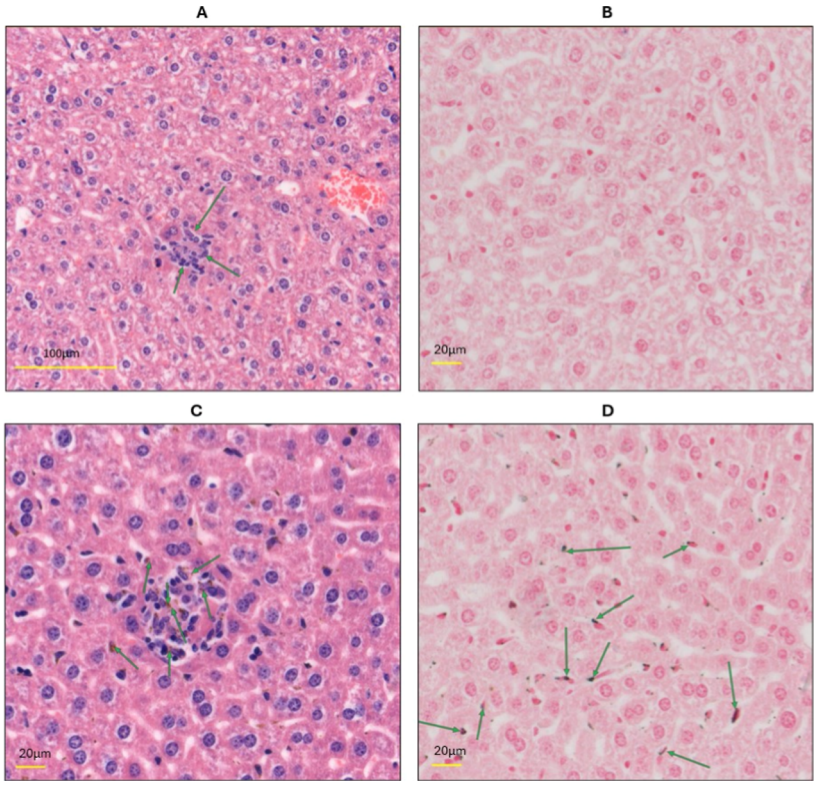

Figure 10. Representative images of H&E and Prussian blue staining of liver sections from SaNP-treated BALB/c mice, 3 days after treatment. (A) H&E-stained liver section from a control (untreated) animal. Green arrows indicate inflammatory cell infiltration. (B) Liver section from a control (untreated) animal stained with PB. No positive pigment accumulation in the Kupffer cells. (C) H&E-stained liver section from a treated animal. Green arrows indicate inflammatory cell infiltration associated with the presence of pigment-laden macrophages. (D) Liver section from a treated animal stained with PB. Green arrows indicate positive pigment accumulation within the Kupffer cells. Scale bars are indicated.

cleaves amide bonds. It is broadly expressed in the liver, heart, skeletal muscle, kidneys, brain, and red blood cells and serves as an index for liver function.[21] Therefore, AST was used as a representative for liver enzymes.

Following enzymatic exposure, physicochemical characterization of SaNPs was conducted by DLS. On two separate repetitions of the experiment all enzyme containing SaNP samples had consistently passed qualitative and quantitative (hydrodynamic size, zeta potential) examinations (Table 2),

Table 2. Physicochemical Characterization of SaNPs Following Enzymatic Exposure

	+SaNP	size (nm)	ZP (mV)	visual inspection
control	WFI	124.7 ± 1.050	−27.1 ± 0.277	brown dispersion without aggregates
treatment	FBS	120.4 ± 2.505	−23.2 ± 0.633	no changes in appearance
	trypsin	113.6 ± 5.441	−26.9 ± 0.383	no changes in appearance
	AST	120.4 ± 6.900	−22.5 ± 0.300	no changes in appearance

without significant changes in their attributes which remained within the specification values described in Table 1. Thus, values in the treated samples compared to the control were similar and the samples were therefore deemed to have preserved their integrity upon enzymatic exposure at stringent conditions.

The physicochemical characteristics of SaNPs were determined by DLS. No particle aggregation was observed in the treatment samples, likewise, there were no deviations in the measured parameters (size and zeta potential; ZP) compared to the control comprised of SaNPs in water for injection (WFI).

4. DISCUSSION

Our previous studies have shown that multicore encapsulated IO SaNPs administered in vivo accumulate in macrophages in the lungs, liver, and spleen,[4,5] which represent the host filtration organs and the main mechanism/s for systemic clearance of nanoparticles by the MPS, in line with others.[21] While in animal studies we did not observe any obvious toxic effects such as necrosis or inflammation, changes in cytotoxicity following SaNP uptake and the underlying molecular mechanisms were not assessed.

Murine RAW264.7 macrophages were used to investigate the cellular response to SaNPs after uptake. The results obtained in this study demonstrate that SaNPs effects in vitro were both time- and dose-dependent. High SaNP concentrations resulted in reduced cell viability of RAW264.7 cells which correlated with the indirect activation of SOD, associated with ROS generation, whereas a low concentration had no effect on cytotoxicity, nor SOD or ROS levels. The enhancement of ROS production induced by nanoparticles depends on the particle size, shape, surface area, and composition. Moreover, the levels of generated ROS, and the resulting oxidative stress, are often correlated with the nanoparticle concentration to which the cells are exposed.

https://doi.org/10.1021/acsomega.4c07883
ACS Omega 2025, 10, 3535−3550

Thus, cells exposed to low concentrations can overcome oxidative stress and recover, whereas cells exposed to higher concentrations activate antioxidant responses leading to cytotoxicity and inflammation.[22]

Regarding the impact of nanoparticle size on ROS production, the study by Huang et al.,[23] found that selenium nanoparticles with a diameter of 81 nm induced more ROS production than other sizes tested (ranging from 43 to 205 nm in diameter). In another study examining the response of monocyte-derived macrophages to the exposure to either titanium dioxide nanoparticles or microparticles with a hydrodynamic size of ∼341 and ∼2112 nm, respectively, a dose-dependent response was observed.[24] The maximum production level of ROS was found upon exposure of these cells to the highest concentration tested (100 μg/mL) of both nanoparticles and microparticles, similar to our concentration range.

Most nanoparticles have a dose-dependent effect, as has been reported for vanadium dioxide nanoparticles[25] and superparamagnetic IO nanoparticles with different surface modifications.[26] The latter also showed that dextran or PEG-coated nanoparticles have reduced toxicity and increased biocompatibility. The cytotoxicity of magnetic nanoparticles with various coatings on cancer cells was also examined,[27] showing that the most significant effect was found in cells treated with unmodified nanoparticles whereas nanoparticle coating increased cell viability, particularly when using PEG 400 or PEG 1000. Feng et al.[28] examined the uptake and toxicity of commercially available IO nanoparticles of varied sizes (10 or 30 nm) and coatings in both macrophage and cancer cells and found that PEGylated nanoparticles were efficiently up taken, exhibited cytotoxicity only at high concentrations and had significantly lower rates of biodegradation and clearance, as supported by our data as well.

Although low SaNP concentrations were not toxic and had no effect on ROS production or SOD activity which was below basal levels, they could stimulate the time-dependent cytokine production of TNF-α by RAW264.7 macrophage cells, indicating SaNP-induced cellular activation, without cytotoxicity, even at low amounts.

Macrophages are able to perform three main functions: (1) removal of pathogens and foreign material, by their elimination through phagocytosis or secretion of antiinfective factors; (2) activation of the immune system, by inducing humoral and cellular immune responses through antigen presentation to T cells and altering the immune microenvironment by releasing various inflammatory agents; and (3) tissue repair, by promoting angiogenesis and the repair of local tissue structure through the release of factors in the late inflammatory stage.[29] The release of TNF-α by RAW264.7 cells following SaNP treatment may reflect the activation of an immune response and/or immune microenvironment modification.

While examining the effect of CM from SaNP-treated RAW264.7 cells on the proliferation of 4T1 cancer cells, we were able to show that CM from SaNP-activated macrophages inhibited 4T1 cell viability, suggesting a SaNP-induced antitumor effect. To further characterize the role of macrophage-secreted soluble factors in this effect, the expression of various cytokines in CM from treated vs untreated RAW264.7 cells was compared, demonstrating increased levels of various factors which included MIP-2, IL-1Ra, ICAM-1, RANTES, and TNF-α released by SaNP-treated macrophages.

MIP-2 is one of the CXC chemokines, also known as chemokine CXC ligand (CXCL2). It affects neutrophil recruitment and activation by binding to chemokine CXC receptor (CXCR)1 and CXCR2 and thereby modulates immune and inflammatory responses. MIP-2 is produced by a variety of cell types, including macrophages, monocytes, epithelial cells, and hepatocytes, in response to infection or injury.[30] MIP-2 has been shown to directly contribute to tumor cell transformation and growth via activation of CXCR2, expressed in cancers with a high metastatic index such as breast, pancreas, ovarian cancer, and melanoma.[31] Although MIP-2 was significantly elevated upon SaNP treatment, it may not be directly involved in the inhibition of cancer cell growth by macrophages but rather seems to be part of their cellular antioxidant response to SaNPs.

An interesting molecule is IL-1Ra, a naturally occurring antagonist of IL-1, which has been shown to possess antitumor activity in mouse B16 melanoma and human melanoma xenograft models, modify the host response to macroscopic tumors, and enhance the antitumor activity of chemotherapeutic drugs.[32] IL-1Ra could potentially impact and inhibit the proliferation of 4T1 cancer cells by SaNP-treated macrophages.

In a study that evaluated the size-dependent cellular interactions of silver nanoparticles with a size between 15 and 55 nm, the activation of the release of several inflammatory mediators was examined by measuring the levels of TNF-α, MIP-2, IL-1b, and IL-6 in the culture media of rat alveolar macrophages.[33] The results demonstrated that after 24 h of exposure, a significant inflammatory response was observed by the release of these cytokines, for all sizes of silver nanoparticles compared to the untreated controls. This study further suggests that the surface area, as well as the size and concentration, play important roles in the nature of the cellular response and contribution to toxicity. Taken together, these data suggest that SaNP-activated macrophage-derived soluble factors promote the inhibition of 4T1 TNBC cells in a paracrine manner. However, these assumptions require further investigation.

The macrophage uptake of FITC-labeled SaNP was verified by several imaging methods offering insight into the uptake and intracellular fate of SaNPs in these cells. The study by Poon et al.[6] examining nanoparticle elimination pathways demonstrated that IV administered nanoparticles mostly interact with Kupffer cells and sinusoidal endothelial cells in the liver which also determine their elimination fate. These non-parenchymal cells in the liver are the primary cells to interact with nanoparticles due to their high phagocytic ability. Kupffer cells were also more effective in the phagocytosis of larger gold nanoparticles (AuNPs) compared to smaller ones (200 and 100 nm, respectively). SaNPs, with a specified size between 90 and 165 nm, were effectively phagocyted by RAW264.7 macrophage cells, and accumulated in the liver after IV administration in both rodents and swine models in vivo.[4,5] Confocal microscopy revealed that SaNPs are effectively internalized after incubation with RAW264.7 cells, appeared to be present in the cytoplasmic compartment and did not enter the nucleus. The cytoplasmic fluorescence had a punctuate pattern, indicating that SaNPs were localized in cellular organelles (e.g., lysosomes) through an endocytic mechanism of internalization. Co-localization of SaNPs within lysosomes was further confirmed by specific staining, using either CytoPainter for lysosomal staining or Prussian blue for

https://doi.org/10.1021/acsomega.4c07883
ACS Omega 2025, 10, 3535−3550

Scheme 1. Schematic Illustration of SaNP-Induced Cellular Responses in Macrophage Cells

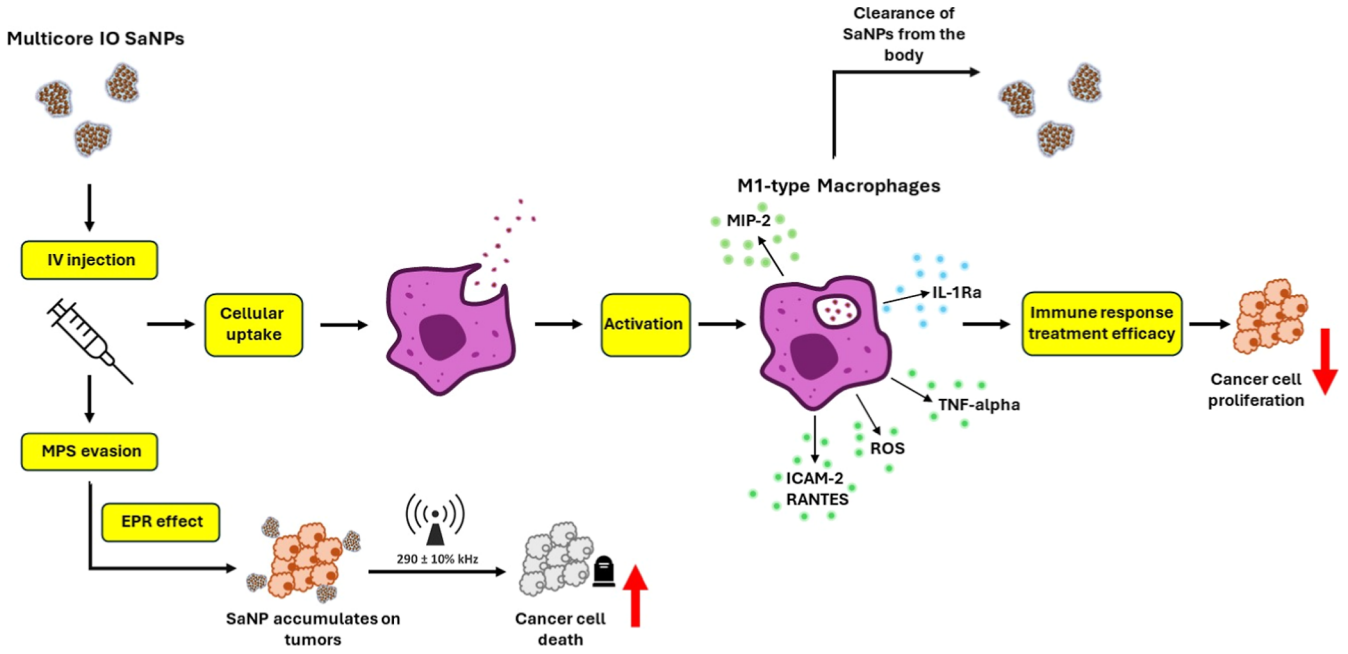

IO-containing SaNPs. Previous studies have suggested that nanoparticles are trafficked to specific cellular organelles. A study that investigated the uptake and intracellular fate of polylactic-*co*-glycolic acid (PLGA) nanoparticles in epithelial cells showed that these nanoparticles colocalized within specific organelles including endosomes, lysosomes, endoplasmic reticulum (ER), and the Golgi apparatus.[34] Moreover, the nanoparticles appeared to colocalize within early endosomes shortly after exposure and were found in other compartments within the cytoplasm, Golgi, and ER over time (4−24 h). Aside from intracellular uptake, the nanoparticles were able to escape endolysosomal degradation and were trafficked to relevant subcellular compartments following endocytosis.

TEM has been widely used to study nanoparticle uptake and cellular localization. The uptake of bare and *N*-(2-aminoethyl)-3-aminopropyltriethoxysilane (aminosilane-APTES)-coated magnetite nanoparticles was evaluated,[35] showing that prostate cancer cells efficiently internalized coated nanoparticles compared to benign cells, further supporting the impact of nanoparticle surface coating. TEM was also used to further confirm the intracellular localization of nanoparticles after macrophage internalization. SaNPs were found to localize in vacuoles and lysosomes, in line with the study by Zhang et al.,[36] which examined the metabolic conversion and removal of manganese (Mn) ferrite nanoparticles in RAW264.7 cells. Both the uptake and cytotoxicity of these nanoparticles in RAW264.7 cells were also time- and dose-dependent. Following their internalization, MnIO nanoparticles underwent sequestration within vacuoles located in the perinuclear region. The pattern of SaNP distribution within the same cells in our case was slightly different, displaying a more homogeneous cytosolic distribution inside the lysosomes, not confined to the vesicles surrounding the nucleus and without entering the nuclei. Interestingly, SaNPs were localized within the mitochondria indicating that they were able to cross the double layered membrane of the mitochondria, which is usually a challenging barrier due to its highly negative potential. This observation requires further investigation. However, Carlson et al.[33] demonstrated that silver nanoparticles could induce alterations in the mitochondrial membrane potential (MMP) in a size-dependent manner, leading to loss of MMP function, suggesting a mechanism of cell death involving mitochondrial-driven apoptosis as the nanoparticles dose or exposure increased, and thus supporting a direct interaction between nanoparticles and the mitochondria.

As indicated by our data, the morphology of the SaNPs, remained unaffected after macrophage phagocytosis and within the size specification range after exposure to proteolytic enzymes, suggesting that they retained their integrity, unlike the MnIO nanoparticles in which the average diameter decreased from the original size following macrophage uptake, indicating that they underwent metabolism and degradation within RAW264.7 cells.[36]

Based on our previous studies in healthy swine,[5] assessing SaNPs' safety and biocompatibility, alone and combined with AMF application, the treatment had no adverse effects, including no negative reactions due to the nanoparticle IV infusion. No noticeable clinical signs were noted during the observation periods, and no inflammation, necrosis, nor thermal damage were found in the histopathology evaluation, supporting lack of treatment-associated toxicities, and suggesting that there was no generation of toxic degradation products of the IO SaNPs.

Imaging flow cytometry analysis was used to quantify the intracellular amounts of FITC- labeled SaNPs up taken and cleared by RAW264.7 cells. When comparing the mean intensity of the FITC-SaNP signals in the examined cells, differences were found between day 0 and the subsequent days 1 and 3, which were significantly reduced, suggesting that most of the SaNPs (∼65%) were removed from the macrophages, during the first 24 h after treatment. Although reduction in signal intensities due to potential degradation should be taken into consideration, the fact that the signal intensities at these time points had a similar decrease compared to the basal levels, could rule out a degradation process because in this case we

https://doi.org/10.1021/acsomega.4c07883
ACS Omega 2025, 10, 3535−3550

would expect a further decrease in the fluorescent signal with time. This is further supported by the microscopy results as well as the histological analysis on day 3, in which no detectable degradation was observed, suggesting that the reduction in the mean intensity of the FITC-SaNP signals observed by flow cytometry is not a result of signal decay due to degradation but stems from time-dependent clearance of the nanoparticles from the macrophage cells.

Degradation depends on the types of enzymes that the nanoparticles encounter during their trajectory inside the body, as well as the chemistry of the coating polymer and the conjugation chemistry by which the nanoparticle components are bound together. We have used a broad set of enzymes to examine the potential in vitro degradation of SaNPs. The results indicated that SaNPs were not degraded at stringent conditions and retained their psychochemical characteristics.

5. CONCLUSIONS

The results obtained in this work demonstrate that multicore encapsulated IO SaNPs induce dose-dependent macrophage activation, as suggested by increased SOD activity and ROS generation induced by high SaNP concentrations. On the other hand, SaNPs induced TNF-α release at lower doses, without cytotoxicity, which could reflect the activation of an immune response and/or immune microenvironment modification, suggesting a potential pro-inflammatory M1 phenotype of the macrophage cells. CM from SaNP-treated macrophage cells induced the inhibition of cancer cell growth suggesting an antitumor effect driven by SaNPs, involving additional cytokines. SaNPs undergo internalization in RAW264.7 cells, promptly localize in the cytosol within lysosomes, and seemingly in the mitochondria, and appear to keep their integrity without intracellular degradation, based on TEM imaging and noncellular enzymatic exposure. Moreover, SaNPs are cleared from the macrophage cells with time in line with previous in vivo studies. A schematic illustration of SaNP-induced cellular responses in macrophage cells is shown in Scheme 1. The unique physicochemical properties of the SaNPs and their design play a key role in these cellular processes and enable their safe use toward clinical application and particularly in cancer therapy.

AUTHOR INFORMATION

Corresponding Author

Sarah Kraus − *New Phase Ltd., Petah Tikva 4951788, Israel;* orcid.org/0000-0003-1083-0297; Phone: +972-3-6545511; Email: sarahk@newphase.co.il; Fax: +972-3-6024439

Authors

Shir Arbib − *New Phase Ltd., Petah Tikva 4951788, Israel*

Pazit Rukenstein − *New Phase Ltd., Petah Tikva 4951788, Israel*

Irit Shoval − *Scientific Equipment Center, the Mina and Everard Goodman Faculty of Life Sciences, Bar Ilan University, Ramat Gan 5290002, Israel*

Raz Khandadash − *New Phase Ltd., Petah Tikva 4951788, Israel*

Ofer Shalev − *New Phase Ltd., Petah Tikva 4951788, Israel*

Complete contact information is available at: https://pubs.acs.org/10.1021/acsomega.4c07883

Author Contributions

S.K. conceptualized the study and designed the experiments. S.K., S.A., and I.S. performed the experiments and the formal analyses. P.R. synthesized the particles and performed the DLS and Zetasizer measurements. R.K. labeled the nanoparticles. S.K. wrote the manuscript with the contributions of S.A., P.R., I.S., R.K., and O.S. O.S. provided the resources and funding. All authors have agreed on the manuscript.

Funding

This work was supported by New Phase Ltd.

Notes

The authors declare the following competing financial interest(s): The authors declare the following competing interests: S. K., S.A., P.R., and O.S. are employees at New Phase Ltd. Other authors declare no conflict of interest.

ACKNOWLEDGMENTS

The authors would like to thank Ekaterina Sigalov for the first investigations into this project, Cheryl Tal for her continuous help and advice, and Ayelet Atkins for her assistance in the TEM studies.

ABBREVIATIONS

AMF, alternating magnetic field; CM, conditioned medium; EIS, electromagnetic induction system; EPR, enhanced permeability and retention; IO, iron oxide; MPS, mononuclear phagocyte system; PCM, phase change material; PEG, polyethylene glycol; ROS, reactive oxygen species; SaNPs, Sarah nanoparticles; SOD, superoxide dismutase; TEM, transmission electron microscopy; TNFα, tumor necrosis factor alpha

REFERENCES

(1) Akbarzadeh, A.; Samiei, M.; Davaran, S. Magnetic nanoparticles: Preparation, physical properties, and applications in biomedicine. *Nanoscale Res. Lett.* **2012**, *7* (1), 144.

(2) Sanità, G.; Carrese, B.; Lamberti, A. Nanoparticle surface functionalization: how to improve biocompatibility and cellular internalization. *Front. Mol. Biosci.* **2020**, *7*, 587012.

(3) Cohen-Erner, M.; Khandadash, R.; Hof, R.; Shalev, O.; Antebi, A.; Cyjon, A.; Kanakov, D.; Nyska, A.; Goss, G.; Hilton, J.; Peer, D. Fe_3O_4 nanoparticles and paraffin wax as phase change materials embedded in polymer matrixes for temperature-controlled magnetic hyperthermia. *ACS Appl. Nano Mater.* **2021**, *4* (10), 11187−11198.

(4) Kraus, S.; Khandadash, R.; Hof, R.; Nyska, A.; Sigalov, E.; Eltanani, M.; Rukenstein, P.; Rabinovitz, R.; Kassem, R.; Antebi, A.; Shalev, O.; Cohen-Erner, M.; Goss, G.; Cyjon, A. Novel nanoparticle-based cancer treatment effectively inhibits lung metastases and improves survival in a murine breast cancer model. *Front. Oncol.* **2021**, *11*, 761045.

(5) Kraus, S.; Rabinovitz, R.; Sigalov, E.; Eltanani, M.; Khandadash, R.; Tal, C.; Rivlin, O.; Sharaga, E.; Rukenstein, P.; Cohen-Erner, M.; Nyska, A.; Siman-Tov, Y.; Shalev, O. Self-regulating novel iron oxide nanoparticle-based magnetic hyperthermia in swine: Biocompatibility, biodistribution, and safety assessments. *Arch. Toxicol.* **2022**, *96*, 2447−2464.

(6) Poon, W.; Zhang, Y. N.; Ouyang, B.; Kingston, B. R.; Wu, J. L. Y.; Wilhelm, S.; Chan, W. C. W. Elimination pathways of nanoparticles. *ACS Nano* **2019**, *13* (5), 5785−5798.

(7) Bene, K.; Halasz, L.; Nagy, L. Transcriptional repression shapes the identity and function of tissue macrophages. *FEBS Open Bio* **2021**, *11*, 3218−3229.

(8) Schieber, M.; Chandel, N. S. ROS function in redox signaling and oxidative stress. *Curr. Biol.* **2014**, *24*, R453−R462.

(9) Singh, R. P.; Ramarao, P. Accumulated polymer degradation products as effector molecules in cytotoxicity of polymeric nanoparticles. *Toxicol. Sci.* **2013**, *136* (1), 131−143.
(10) Zhang, M.; Yang, M.; Bussy, C.; Iijima, S.; Kostarelos, K.; Yudasaka, M. Biodegradation of carbon nanohorns in macrophage cells. *Nanoscale* **2015**, *7* (7), 2834−2840.
(11) McLennan, H. R.; Esposti, M. D. The contribution of mitochondrial respiratory complexes to the production of reactive oxygen species. *J. Bioenerg. Biomembr.* **2000**, *32* (2), 153−162.
(12) Zhu, L.; Pelaz, B.; Chakraborty, I.; Parak, W. J. Investigating possible enzymatic degradation on polymer shells around inorganic nanoparticles. *Int. J. Mol. Sci.* **2019**, *20* (4), 935.
(13) van Horssen, R.; Ten Hagen, T. L.; Eggermont, A. M. TNF-alpha in cancer treatment: Molecular insights, antitumor effects, and clinical utility. *Oncologist* **2006**, *11* (4), 397−408.
(14) Canton, M.; Sánchez-Rodríguez, R.; Spera, I.; Venegas, F. C.; Favia, M.; Viola, A.; Castegna, A. Reactive oxygen species in macrophages: Sources and targets. *Front. Immunol.* **2021**, *12*, 734229.
(15) Geng, Y.; Hardie, J.; Landis, R. F.; Mas-Rosario, J. A.; Chattopadhyay, N. A.; Keshri, P.; Sun, J.; Rizzo, E. M.; Gopalakrishnan, S.; Farkas, M. E.; Rotello, V. M. High-content and high-throughput identification of macrophage polarization phenotypes. *Chem. Sci.* **2020**, *11* (31), 8231−8239.
(16) Zhang, Z.; Yue, P.; Lu, T.; Wang, Y.; Wei, Y.; Wei, X. Role of lysosomes in physiological activities, diseases, and therapy. *J. Hematol. Oncol.* **2021**, *14* (1), 79.
(17) Luo, W.; Liu, R. S.; Zhu, G. J.; Li, Y. C.; Liu, H. C. Subcellular location and photodynamic therapeutic effect of chlorin e6 in the human tongue squamous cell cancer Tca8113 cell line. *Oncol. Lett.* **2015**, *9* (2), 551−556.
(18) Dominical, V.; Samsel, L.; McCoy, Jr J. P. Masks in imaging flow cytometry. *Methods* **2017**, *112*, 9−17.
(19) Palazzi, X.; Burkhardt, J. E.; Caplain, H.; Dellarco, V.; Fant, P.; Foster, J. R.; Francke, S.; Germann, P.; Gröters, S.; Harada, T.; Harleman, J.; Inui, K.; Kaufmann, W.; Lenz, B.; Nagai, H.; Pohlmeyer-Esch, G.; Schulte, A.; Skydsgaard, M.; Tomlinson, L.; Wood, C. E.; Yoshida, M. Characterizing "adversity" of pathology findings in nonclinical toxicity Studies: Results from the 4th ESTP International Expert Workshop. *Toxicol. Pathol.* **2016**, *44* (6), 810−824.
(20) Cottrell, G. S.; Amadesi, S.; Grady, E. F.; Bunnett, N. W. Trypsin IV, a novel agonist of protease-activated receptors 2 and 4. *J. Biol. Chem.* **2004**, *279* (14), 13532−13539.
(21) McGill, M. R. The past and present of serum aminotransferases and the future of liver injury biomarkers. *EXCLI J.* **2016**, *15*, 817−828.
(22) Gustafson, H. H.; Holt-Casper, D.; Grainger, D. W.; Ghandehari, H. Nanoparticle uptake: The phagocyte problem. *Nano Today* **2015**, *10* (4), 487−510.
(23) Huang, T.; Holden, J. A.; Heath, D. E.; O'Brien-Simpson, N. M.; O'Connor, A. J. Engineering highly effective antimicrobial selenium nanoparticles through control of particle size. *Nanoscale* **2019**, *11* (31), 14937−14951.
(24) Kheder, W.; Soumya, S.; Samsudin, A. R. Impact of titanium dioxide particle size on macrophage production of intracellular reactive oxygen species. *Arch. Oral Biol.* **2021**, *127*, 105133.
(25) Xi, W. S.; Tang, H.; Liu, Y. Y.; Liu, C. Y.; Gao, Y.; Cao, A.; Liu, Y.; Chen, Z.; Wang, H. Cytotoxicity of vanadium oxide nanoparticles and titanium dioxide-coated vanadium oxide nanoparticles to human lung cells. *J. Appl. Toxicol.* **2020**, *40* (5), 567−577.
(26) Mojica Pisciotti, M. L.; Lima Jr, E.; Vasquez Mansilla, M.; Tognoli, V. E.; Troiani, H. E.; Pasa, A. A.; Creczynski-Pasa, T. B.; Silva, A. H.; Gurman, P.; Colombo, L.; Goya, G. F.; Lamagna, A.; Zysler, R. D. In vitro and in vivo experiments with iron oxide nanoparticles functionalized with dextran or polyethylene glycol for medical applications: Magnetic targeting. *J. Biomed. Mater. Res. B Appl. Biomater.* **2014**, *102* (4), 860−868.
(27) Zavisova, V.; Koneracka, M.; Kovac, J.; Kubovcikova, M.; Antal, I.; Kopcansky, P.; Bednarikova, M.; Muckova, M. The cytotoxicity of iron oxide nanoparticles with different modifications evaluated in vitro. *J. Magn. Magn. Mater.* **2015**, *380*, 85−89.
(28) Feng, Q.; Liu, Y.; Huang, J.; Chen, K.; Huang, J.; Xiao, K. Uptake, distribution, clearance, and toxicity of iron oxide nanoparticles with different sizes and coatings. *Sci. Rep.* **2018**, *8* (1), 2082.
(29) Ding, X.; Sun, X.; Cai, H.; Wu, L.; Liu, Y.; Zhao, Y.; Zhou, D.; Yu, G.; Zhou, X. Engineering macrophages via nanotechnology and genetic manipulation for cancer therapy. *Front. Oncol.* **2022**, *11*, 786913.
(30) Qin, C. C.; Liu, Y. N.; Hu, Y.; Yang, Y.; Chen, Z. Macrophage inflammatory protein-2 as mediator of inflammation in acute liver injury. *World J. Gastroenterol.* **2017**, *23* (11), 3043−3052.
(31) Erin, N.; Nizam, E.; Tanrıöver, G.; Köksoy, S. Autocrine control of MIP-2 secretion from metastatic breast cancer cells is mediated by CXCR2: a mechanism for possible resistance to CXCR2 antagonists. *Breast Cancer Res. Treat.* **2015**, *150* (1), 57−69.
(32) Triozzi, P. L.; Aldrich, W. Effects of interleukin-1 receptor antagonist and chemotherapy on host−tumor interactions in established melanoma. *Anticancer Res.* **2010**, *30* (2), 345−354.
(33) Carlson, C.; Hussain, S. M.; Schrand, A. M.; Braydich-Stolle, L. K.; Hess, K. L.; Jones, R. L.; Schlager, J. J. Unique cellular interaction of silver nanoparticles: Size-dependent generation of reactive oxygen species. *J. Phys. Chem. B* **2008**, *112*, 13608−13619.
(34) Cartiera, M. S.; Johnson, K. M.; Rajendran, V.; Caplan, M. J.; Saltzman, W. M. The uptake and intracellular fate of PLGA nanoparticles in epithelial cells. *Biomaterials* **2009**, *30* (14), 2790−2798.
(35) Youhannayee, M.; Nakhaei-Rad, S.; Haghighi, F.; Klauke, K.; Janiak, C.; Ahmadian, M. R.; Rabenalt, R.; Albers, P.; Getzlaff, M. Physical characterization and uptake of iron oxide nanoparticles of different prostate cancer cells. *J. Magn. Magn. Mater.* **2019**, *473*, 205−214.
(36) Zhang, L.; Xiao, S.; Kang, X.; Sun, T.; Zhou, C.; Xu, Z.; Du, M.; Zhang, Y.; Wang, G.; Liu, Y.; Zhang, D.; Gong, M. Metabolic conversion and removal of manganese ferrite nanoparticles in RAW264.7 cells and induced alteration of metal transporter gene expression. *Int. J. Nanomed.* **2021**, *16*, 1709−1724.

https://doi.org/10.1021/acsomega.4c07883
ACS Omega 2025, 10, 3535−3550